J Neurophysiol
88: 1363–1373, 2002; 10.1152/jn.00967.2001.

Contrast-Dependent Changes in Spatial Frequency Tuning of Macaque V1 Neurons: Effects of a Changing Receptive Field Size

MICHAEL P. SCENIAK,[1,2] MICHAEL J. HAWKEN,[2] AND ROBERT SHAPLEY[2]
[1]*University of California, Davis California 95616; and* [2]*Center for Neural Science, New York University, New York, New York 10003*

Received 26 November 2001; accepted in final form 29 May 2002.

Sceniak, Michael P., Michael J. Hawken, and Robert Shapley. Contrast-dependent changes in spatial frequency tuning of macaque V1 neurons: effects of a changing receptive field size. *J Neurophysiol* 88: 1363–1373, 2002; 10.1152/jn.00967.2001. Previous studies on single neurons in primary visual cortex have reported that selectivity for orientation and spatial frequency tuning do not change with stimulus contrast. The prevailing hypothesis is that contrast scales the response magnitude but does not differentially affect particular stimuli. Models where responses are normalized over contrast to maintain constant tuning for parameters such as orientation and spatial frequency have been proposed to explain these results. However, our results indicate that a fundamental property of receptive field organization, spatial summation, is not contrast invariant. We examined the spatial frequency tuning of cells that show contrast-dependent changes in spatial summation and have found that spatial frequency selectivity also depends on stimulus contrast. These results indicate that contrast changes in the spatial frequency tuning curves result from spatial reorganization of the receptive field.

INTRODUCTION

According to previous studies of visual responses in mammalian primary visual cortex, V1, orientation, and spatial frequency tuning of single V1 neurons do not change with stimulus contrast (Albrecht and Hamilton 1982; Bradley et al. 1987; Li and Creutzfeldt 1984; Movshon et al. 1978; Sclar and Freeman 1982; Sclar et al. 1990; Skottun et al. 1987). Contrast normalization has been introduced as a mechanism to account for response scaling with contrast without changing the response tuning for spatial parameters like orientation and spatial frequency (Bonds 1989; Heeger 1992; Ohzawa et al. 1985).

Recently, it has been shown that the interactions between the "classical" receptive field of a V1 neuron and its surroundings are influenced by the contrast adaptation state of the neuron (Kapadia et al. 1999; Levitt and Lund 1997; Sceniak et al. 1999). Not only is the classical receptive field's responsiveness influenced by contrast, but so too is its spatial extent (Sceniak et al. 1999). Therefore the contrast adaptation state of the neuron alters the spatial properties of the receptive field in a way that is more complex than simply scaling the gain. We investigated whether other spatial properties of the receptive field might be dependent on the contrast adaptation state of the neuron. To do this we examined the spatial frequency tuning of V1 cells that show contrast-dependent changes in spatial summation. The result of these experiments is that spatial frequency selectivity also depends on stimulus contrast. Spatial frequency tuning bandwidth is consistently smaller at low contrast than at high contrast (our findings agree with some of the data of Bradley et al. 1987 on cat visual cortex but not with the paper's summary and conclusions). The reduction occurs predominately on the high end of the spatial frequency tuning curve. Spatial frequency preference is relatively unaffected by contrast.

By considering models for signal combination in cortical cells, one can make predictions about whether the previously observed changes in spatial summation (Sceniak et al. 1999) are related to the contrast-dependent changes in spatial frequency selectivity. Changes in spatial summation along the length axis should not affect the spatial frequency characteristics, although such changes may influence the orientation tuning bandwidth. Changes in width summation might be expected to affect spatial frequency tuning. The effects may involve either a widening of each subunit of the receptive field or an increase in the number of subunits of a fixed size.

Simple cell receptive fields have been modeled as a Gabor filter followed by a static nonlinearity (Daugman 1980, 1984, 1985; DeAngelis et al. 1991, 1993; Field and Tolhurst 1986; Jones and Palmer 1987; Kulikowski et al. 1982; Marcelja 1980; Stork and Wilson 1990). A model with multiple spatially overlapping linear Gabor filters that are rectified and then pooled as a spatial sum has been used to describe complex cells (Emerson et al. 1987; Glezer et al. 1980; Heggelund 1981; Movshon et al. 1978b; Spitzer and Hochstein 1985a,b, 1988; Szulborski and Palmer 1990). For either simple or complex cells, the linear first stage filters' spatial properties determine the spatial frequency tuning (preference and selectivity) of the neuron (Spitzer and Hochstein 1988). If the spatial envelope of the impulse response of a Gabor filter increases keeping the subunit size constant, the bandwidth of the frequency response decreases and vice versa (Fig. 1, *A* and *B*). This property holds for both the simple cell and complex cell models.

Although the Gabor filter model seems to describe the basic subunit structure of a cortical simple cell, it suffers from several limitations. First of all, in such a model the receptive field subregions are all spatially identical. This is the result of

Address for reprint requests: M. P. Sceniak, Center for Neuroscience, University of California Davis, 1544 Newton Ct., Davis, CA 95616 (E-mail: mpsceniak@ucdavis.edu).

The costs of publication of this article were defrayed in part by the payment of page charges. The article must therefore be hereby marked "*advertisement*" in accordance with 18 U.S.C. Section 1734 solely to indicate this fact.

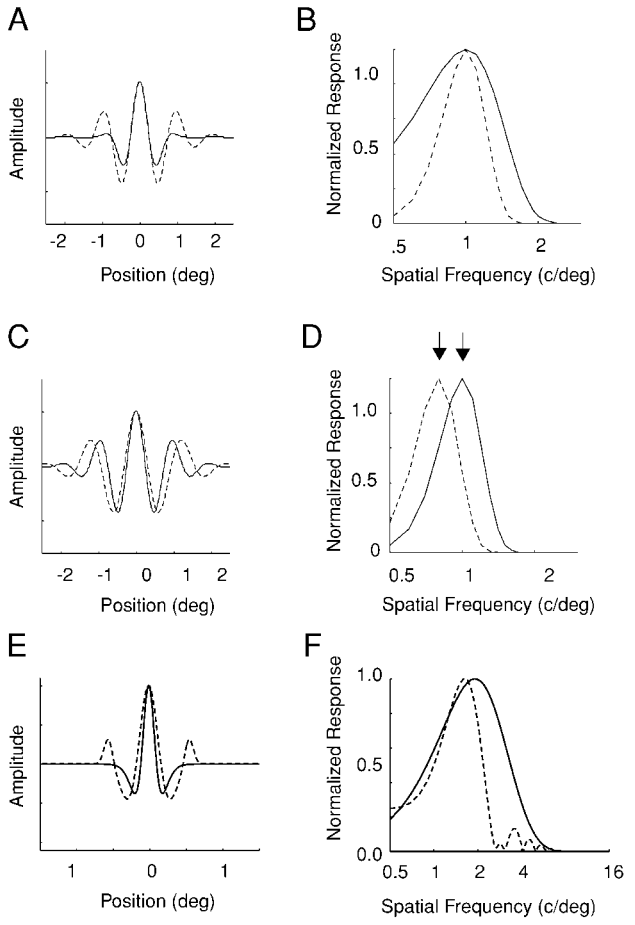

FIG. 1. Gabor filter model of a receptive field. Gabor filters were tested with sinusoidal inputs varying in spatial frequency to compare the spatial frequency tuning for particular perturbations in the model parameters. *A*: one-dimensional (1D) spatial profiles for the linear filter used to compute spatial frequency tuning in a model simple cell. Solid curve presents the spatial profile for a Gabor filter with sinusoidal frequency of 1 cycle/° and a Gaussian envelope of 0.8°. Dashed curve shows the spatial profile for a Gabor filter composed of a 1 cycle/° sine wave and a 1.6° Gaussian envelope. The extent of summation for the solid profile is smaller than that of the dashed profile. *B*: spatial frequency tuning curves calculated from the profiles in *A*. The Gabor filter with the wider Gaussian envelope (dashed curve) produces narrower spatial frequency tuning. In addition to changing the Gaussian envelope spread, the carrier frequency of the Gabor filter could be modified. *C*: spatial impulse response of 2 simulated receptive fields. The solid and dotted curves represent Gabor filters with carrier frequencies of 1 and 0.8 cycles/°, respectively. In both filters, the Gaussian envelope is of the same size (1.6°). *D*: spatial frequency response for the 2 filters shown in *C*. Vertical arrows indicate the peak spatial frequency tuning for each filter. Notice that the filter with the narrower subunits (solid curve) shows a higher peak tuning than the filter with broader subunits (dotted curve), but that the bandwidth is the same for the 2 filters. More complex changes can result when the spatial profile is modeled as a difference of Gaussian (DOG) with flanking subunits rather than as a Gabor filter. *E*: solid curve illustrates a spatial profile resulting from a DOG. The dashed curve is a DOG with a wider central subunit and the addition of flanking Gaussian subunits. The spatial profile resembles a Gabor filter; however, the subunits are not all equal in spatial spread. *F*: spatial frequency tuning curves resulting from spatial profiles in *E*. Increased spatial spread of the central subunit in the DOG and flanking subunits produce a reduction of the high spatial frequencies (dashed curve) when compared with the frequency response of the original DOG spatial profile (solid curve).

modeling all of the subunits with a single sine or cosine function. Moreover, the bandwidth reduction of the Gabor filter when its envelope is increased in width must be symmetric about the peak spatial frequency, contrary to what we observed. Therefore the contrast-dependent changes in spatial frequency tuning we observed could not be easily modeled by adjusting the parameters of Gabor filters.

It has been shown previously that V1 simple cells are better described by difference of Gaussian (DOG) functions than by Gabor functions (Hawken and Parker 1987). One advantage of the DOG model is that it allows for independent manipulation of subunit size and strength. The DOG model provides a wider range of possible changes in the spatial frequency tuning than the Gabor model (Wallis 2002). If the receptive field is modeled as a DOG with two flanking Gaussian subunits, the resulting profile resembles a Gabor filter with the added feature that we can alter independently the height and spread of the subunits. By increasing the spread of the center Gaussian and also increasing the strength of flanking Gaussians, we can produce a spatial filter with a reduction in response amplitude only at high spatial frequencies and little change in the spatial frequency preference (Fig. 1, *E* and *F*). This is the nature of the change we observe in V1 neurons' spatial frequency tuning when contrast is reduced (shown in RESULTS).

METHODS

Standard electrophysiological recording techniques were used in acute preparation of macaque monkeys (Hawken et al. 1996, Sceniak et al. 2001). Extracellular action potentials were collected from isolated single neurons using extracellular microelectrodes. Spikes were analyzed both during experiments and off-line, using standard software packages and custom software written specifically for this purpose. Details of the procedures used in the experiments and the data analysis are given below.

Animal preparation

Acute experiments were performed on adult Old World monkeys (*Macaca fascicularis*) in strict compliance with the guidelines for humane care and use of laboratory animals published by National Institutes of Health and Public Health Service. Animals were initially tranquilized with acepromazine (50 μg/kg, im). After administering the tranquilizer (approximately 15 min), we anesthetized the animal with ketamine (30 mg/kg, im). Additional ketamine was given as needed during the initial phase of surgery. Venous cannulation and tracheotomy were carried out under ketamine, and we then transferred to an opioid anesthetic sufentanyl (sufentanyl citrate, 6 μg/kg/h, iv) and maintained anesthesia throughout the experiment with sufentanyl. A broad spectrum antibiotic (Bicillin, 50,000 iu/kg, im) and anti-inflammatory steroid (dexamethasone, 0.5 mg/kg, im) were given at the initial surgery and every other day during the recording period. Anesthesia level was determined by analysis of the EEG waveform, heart rate, blood pressure, and CO_2 output. Anesthetic state was judged to be satisfactory if there was predominant slow wave EEG activity and if potentially mildly noxious stimuli produced no change in EEG, heart rate, or blood pressure. Expired CO_2 was maintained close to 5%. Rectal temperature was monitored and kept at a constant 37.5°C. A small craniotomy was performed over the striate cortex for recording. Across animals, the craniotomies were positioned so that the recorded receptive fields displayed a parafoveal eccentricity between 2 and 5° of visual angle. Anesthesia was administered throughout the recording period with sufentanyl (6 μg/kg/h, iv) and paralysis was induced with pancuronium bromide (0.1 mg/kg/h, iv). The anesthetic and paralytic were administered in balanced physiological solution at a rate of 10–20 ml/h. Experiments were terminated with a lethal dose of pentobarbital (60 mg/kg, iv). The animal was perfused through the heart with a mixture of heparinized saline followed by 2 liters of fixative (4% paraformaldehyde in phosphate buffer, pH 7.4)

for later histological reconstruction. Histological reconstruction was performed using the same methods as described in Hawken et al. (1988, 1996).

Optics

The eyes were initially treated with 1% atropine sulfate solution to dilate the pupils. The eyes were protected by gas-permeable contact lenses. Prior to adding the lenses, the eyes were treated with a topical antibiotic (gentamicin sulfate, 3%). Foveae were mapped onto a tangent screen using a reversing ophthalmoscope (Eldridge 1979). The visual receptive fields of isolated neurons were mapped on the same tangent screen, keeping reference to the foveae. Proper refraction was achieved by placing corrective lenses mounted in front of the eyes on custom designed lens holders. Refraction adjustments were made during the recording session by stimulating a responsive cell with a grating with a spatial frequency near the cutoff frequency. The lens power was adjusted to produce a maximal response.

Extracellular recording

The electrode was advanced through the gray matter via a stepping motor (1-μm step size) mounted to a microdrive (Narashige, Japan). Single unit recordings were made with glass-coated tungsten microelectrodes with exposed tips of 5–15 μm (Merrill and Ainsworth 1972). The signal was amplified using a Dagan (MN) EX4–400 differential amplifier and band-pass filtered (0.1–10 kHz). This analog signal was then sent to an A/D signal processing board of a digital computer (SGI, Mountain View, CA). Spikes were discriminated and time-stamped using software custom designed for this purpose and running on a Silicon Graphics O2 computer. Single spikes were isolated from the recording, using tailored waveform windowing. Spikes were time stamped with an accuracy of 1 ms. Strict criteria for single-unit recording included fixed shape of the action potential and the absence of spikes during the absolute refractory period.

Experimental protocol

All of the experiments discussed here were conducted using drifting sinusoidal gratings. The optimal stimulus parameters for orientation, size, and temporal frequency were estimated prior to conducting the following experiments. These optimal parameters were used to generate grating stimuli for the spatial frequency experiments. Sinusoidal drifting gratings of the preferred orientation and temporal frequency were presented centered over the receptive field. Each stimulus presentation lasted 4 s. Ten spatial frequencies ranging from 0.1 cycles/° to slightly above the cell's cutoff frequency were presented randomly in logarithmic steps. The contrast was routinely set to be high during these experiments (64–90%). During the characterization of each cell's color properties, we collected spatial frequency response curves using cone isolating stimuli as well as equiluminant red-green and luminance stimuli that were set to the same cone contrast. Cone contrast was equal to the maximal achievable cone contrast of our monitor for equiluminant red-green stimuli (equivalent to 20% luminance contrast). Therefore spatial frequency tuning curves for luminance (black-white) stimuli were estimated at a fixed low (20%) and high contrast (64–90%) for each cell.

In separate experiments, to estimate the spatial frequency bandwidth more accurately, spatial frequency was sampled more densely. Drifting sine wave gratings were presented in a rectangular aperture (4° square) oriented parallel to the cell's preferred orientation and centered over the excitatory receptive field. For cells that exhibit substantial end inhibition (50% or more), the rectangle's length was reduced to exclude the inhibitory zone along the length, but the width was kept fixed at 4°. Each grating patch size was presented for 4 s. Blanks (4 s) of the same mean luminance as the grating stimuli were presented interleaved with grating stimuli to determine the spontaneous firing rate and to avoid response adaptation. The spatial frequency of the drifting grating was varied in a random order. Spatial frequency was sampled logarithmically using 10–12 spatial frequencies centered around the preferred spatially frequency (estimated from previous experiments). The low and high cutoff frequencies were tailored to each cell based on previous spatial frequency characterizations as discussed above. Three repeats of the response to each spatial frequency were collected. By collecting several points around the peak spatial frequency, we were able to make precise estimates of the spatial frequency bandwidth of each cell.

We repeated this procedure at two contrast levels. The contrast levels were taken from the sloping region of the contrast response function of each cell. Therefore the contrast levels are chosen based on the cell's response. Low contrasts were chosen such that they were near the low end of the contrast response function, but elicited responses that were significantly greater than the spontaneous firing rate (2 SDs or more). High contrasts were selected to elicit responses that were $<$90% of the saturation response for each cell.

Each cell was also tested for spatial summation at multiple contrast levels. The center of the receptive field was carefully located using a small (0.2° diam) circular grating patch. Once the center was located, circular patches of drifting sinusoidal grating were presented and centered over the receptive field. Each grating patch size was presented for 4 s. Four-second blanks of the same mean luminance as the grating stimuli were presented interleaved with grating stimuli to determine the spontaneous firing rate and to avoid response adaptation. The patch sizes were presented in a random order. The radius ranged from 0.1° to 5° of visual angle in logarithmic steps. Each summation curve consisted of 10 radii with two repeats at each size. Contrast levels were held constant during repeats to avoid effects of adaptation. Outside each patch, the rest of the screen (12° $\times$ 17° visual angle) was kept at the mean luminance of 56 cd/m^2. The contrast levels chosen for low and high contrasts were identical to those used in the spatial frequency experiments.

We repeated the summation experiment using rectangular patches that extend independently in the length or width dimension. The patch length was varied randomly in the same manner described above for the circular patch summation experiments. Then we conducted a similar experiment by varying the width in a similar random fashion. Therefore we acquired area, length, and width summation curves at two contrast levels in three temporally separated experiments.

Receptive field model simulations

To determine the possible interactions of contrast on the receptive field spatial substructure, we modeled the spatial frequency responses of a theoretical neuron. This was accomplished by two separate models. First, we used a Gabor filter (Daugman 1980, 1984, 1985; Kulikowski et al. 1982). Next, we repeated the simulation with a model comprised of a difference of Gaussians with flanking Gaussian subunits (Hawken and Parker 1987).

The spatial impulse response of the Gabor filter, $g(x)$, is defined as

$$g(x) = R_0 + Le^{-(x-D)^2/2\lambda^2} \cos(2\pi sf(x - D) + \phi)$$

The parameter, R_0, is the spontaneous firing rate, L is the gain, D is the spatial phase offset of the envelope, sf is the carrier frequency of the Gabor, λ is the space constant of the Gaussian envelope, and ϕ is the subunit spatial phase offset.

For a given spatial stimulus input, $s(x)$, where

$$s(x) = \cos(2\pi\omega x)$$

is convolved with a Gabor filter, $g(x)$. In the Fourier domain, the output, $O(\omega)$ is

$$\hat{O}(\omega) = \hat{S}(\omega) \cdot \hat{G}(\omega)$$

where $S(\omega)$ and $G(\omega)$ are the Fourier transform of the input signal $s(x)$ and the Gabor filter $g(x)$, respectively. The convolved input signal is then subjected to a static nonlinear threshold such that the output is given by

$$\hat{O}(\omega) = \max(\hat{S}(\omega) \cdot \hat{G}(\omega), 0)$$

For simple cells, the first harmonic response is calculated for this output over a range of input spatial frequencies to yield the simulated spatial frequency tuning curve. Similar analysis can be used for complex cells. In this case the subunit structure is composed of multiple overlapping Gabor filters that are separated by a phase offset. Each first stage filter is initially convolved with the input and rectified by the threshold nonlinearity then the responses are pooled. The spatial frequency responses of the complex cells are dominated by the initial linear filter stage in agreement with previous reports (Spitzer and Hochstein 1985a,b).

To determine the effects of nonuniform subunits, receptive fields were also modeled as a difference of Gaussians (DOG) with flanking Gaussians (Fig. 1, *E* and *F*). Here the central subunit is modeled as a DOG defined by

$$g(x) = M_e e^{(-(x)^2)/2\alpha^2} - M_i e^{(-(x)^2)/2\beta^2}$$

where M_e and M_i are the sensitivities of the center and surround of the central DOG subregion and α and β are their space constants. The flanking Gaussians are defined by

$$s(x) = Ne^{(-(x-\varepsilon)^2)/2\xi^2} + Ne^{(-(x+\varepsilon)^2)/2\xi^2}$$

where N is the sensitivity, ϵ is the spatial displacement of the flanking subunits from the center, and ξ is their space constant. The resulting spatial profile would be the sum

$$r(x) = g(x) + s(x)$$

Spatial frequency responses were estimated by convolving the spatial impulse response $r(x)$ with sinusoids over a range of frequencies.

Data analysis

To quantify the spatial frequency responses, each tuning curve was fitted using the following empirical function

$$R(sf) = R_0 + P_e e^{-((sf-\mu)/2\sigma_e^2)^2} - P_i e^{-((sf-\mu)/2\sigma_i^2)^2}$$

Here, R_0, is the spontaneous rate estimated from the blank presentations. Values of P_e, P_i, σ_e, σ_I, and μ were optimized to provide the least squared error fit to the data. This function is a difference of Gaussians. The spatial frequency peak and bandwidth were estimated empirically from the fitted curves for low and high contrast. Peak spatial frequency was taken as the spatial frequency that elicits maximal response.

Bandwidth estimates were estimated as the log ratio (in octaves) of the spatial frequencies that elicited half the maximal response for the high-frequency cutoff to the low-frequency cutoff [$\log_2(SF_{high\ cutoff}/SF_{low\ cutoff})$]. Bandwidth and peak spatial frequency estimates were taken from the fitted curves for the first harmonic response of simple cells and the DC response of complex cells.

Spatial summation tuning curve analysis

Each spatial summation curve was fitted using the following empirical function

$$R(s) = R_0 + K_e \int_{-s/2}^{s/2} e^{-(2y/a)^2} dy - K_i \int_{-s/2}^{s/2} e^{-(2y/b)^2} dy$$

Here, R_0 is the spontaneous rate, and each integral represents the relative contribution from putative excitatory and inhibitory components respectively (Sceniak et al. 1999, 2001). Values of K_e, a, K_i, and b were optimized to provide the least squared error fit to the data. Excitatory space constant measures are taken as the parameter a from the fitted curves for the first harmonic response of simple cells and the DC response of complex cells.

Iceberg analysis

To determine the effects of a response threshold on low contrast responses, we simulated the "iceberg" effect on the empirical data. The point of the simulation is to compare the actual empirical responses collected at low contrast to those simulated from the high contrast responses. Initially the spontaneous firing rate was subtracted from both the high and low contrast responses. The iceberg responses at low contrast were constructed by subtracting the difference between the peak response at high − low contrast. This produced responses that are matched in peak response by a linear scaling assumed from the contrast response function. Next, the iceberg responses are subjected to a response threshold at 0 spikes/s. The resulting iceberg responses are the prediction of the low contrast responses. These responses are compared with the actual empirical responses at low contrast.

RESULTS

Spatial frequency tuning at low and high contrast

We compared the spatial frequency response function at low and high contrast (Fig. 2, *A* and *B*). For a significant number of cells, reducing the contrast causes a reduction in the spatial frequency bandwidth (Fig. 2, *A* and *B*). However, the spatial frequency peak is relatively unaffected by contrast. Normalizing the response magnitude to equate the response peaks makes the change in spatial frequency bandwidth more obvious. While some cells show equal reduction on both ends of the spatial frequency tuning curve (Fig. 2*A*), more cells show a reduction which is stronger on the high end of the tuning curve (Figs. 2*B* and 3). Therefore there is a bias toward preserving low frequencies and reducing the response to high frequencies as contrast is reduced.

Population estimates of spatial frequency selectivity at low and high contrast

In our initial study, we collected spatial frequency tuning curves at high (64–99% contrast) and low (20%) contrast, using optimal drifting gratings in a circular aperture. Our sample population includes only those cells that gave responses that were significantly above the spontaneous firing rate (>2 SDs above the spontaneous firing rate and more than 10 spikes/s) and had a maximum response well below response saturation (90% or less of the saturating response as judged from the contrast response function). Each spatial frequency response was fitted with a difference of Gaussians (DOG) empirical function (see METHODS). The spatial frequency optimal value was taken as the spatial frequency eliciting maximal response from the fitted DOG curves. Bandwidth estimates were taken as the log ratio (in octaves) of the spatial frequencies that produced responses that were one-half of the maximum response on either side of the peak (the ratio was defined as the $\log_2$ of the high cutoff frequency to the low cutoff frequency, $SF_{high\ cutoff}/SF_{low\ cutoff}$). Mean spike rates were used

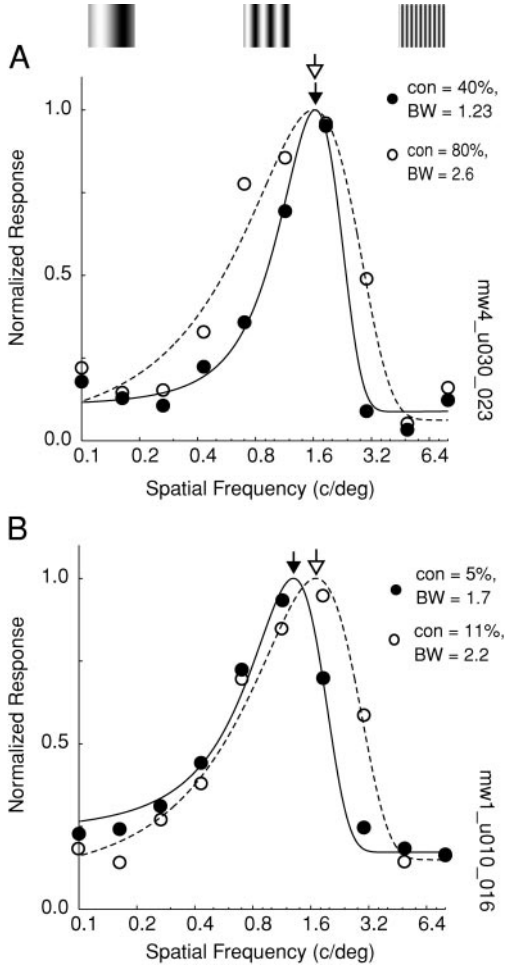

FIG. 2. Spatial frequency tuning at high and low contrast. Responses for high contrast stimuli are indicated by open circles and low contrast stimuli by closed circles. Responses were fitted with a difference of Gaussians curve. Dashed curve indicates the high contrast fit and the solid curve the low contrast fit. Open and closed arrows indicate the response peak for high and low contrast responses, respectively. *A*: spatial frequency tuning that shows a symmetric change in spatial frequency bandwidth (BW_{low} = 1.23 octaves, BW_{high} = 2.6 octaves). *B*: representative neuron that shows a reduction in the spatial frequency bandwidth (BW_{low} = 1.7 octaves, BW_{high} = 2.2 octaves) with contrast most of which can be accounted for by a reduction in responses to high spatial frequencies. There is a small shift in peak spatial frequency.

for complex cells and first harmonic responses for simple cells. Across the population ($n = 47$, cells with peak spatial frequencies at low contrast below 0.4 c/° were excluded), bandwidth estimates are greater at high contrast than low contrast for both simple and complex cells (Fig. 3*A*). The mean bandwidth ratio for high to low contrast (BW_{high}/BW_{low}) is 1.24 (the mean is significantly different from unity, Wilcoxon ranked sum test, $P < 0.01$, Fig. 3*C*) indicating that the bandwidth is roughly 24% larger at high contrast. For the same population of cells ($n = 47$), although there is not significant difference in the ratio of spatial frequency peak at high to the peak at low contrast (the mean of the ratios is not statistically different from unity, $P > 0.05$, Wilcoxon ranked sum test, Fig. 3*D*), there is a slight trend for peak spatial frequency to be higher at high contrast ($Peak_{high}/Peak_{low} = 1.10$). Cells showing the largest changes in spatial frequency bandwidth are located predominantly in the lower layers, layers 5 and 6 (Fig. 4*A*).

Initially, all spatial frequency estimates for the cells in Fig. 3, *A* and *B* were made at a fixed low contrast (20%). To compare contrast-dependent spatial summation changes to the spatial frequency changes presented here, we collected spatial frequency tuning curves at the same contrast used to estimate spatial summation ($n = 19$). This reduced population shows a similar trend for spatial frequency bandwidth at high to low contrast ($BW_{high}/BW_{low} = 1.7$, Fig. 3*E*) and the population mean is significantly different from unity (Wilcoxon ranked sum test, $P < 0.01$). Spatial frequency peak or optimal tuning does not vary significantly with contrast ($BW_{high}/BW_{low} = 1.10$), and the mean is not significantly different from unity ($P > 0.05$, Wilcoxon ranked sum test, Fig. 3*F*). The contrast-dependent change in spatial frequency tuning bandwidth is also seen in the lower layers in the small sample (Fig. 4*B*), but we did not sample enough cells in the middle and upper layers to determine the prevalence of contrast-dependent changes in those layers ($n = 14$). There are fewer cells in Fig. 4*A* than Fig. 3, *E* and *F*, because not all cells could be assigned a laminar position from the histological reconstruction procedure.

For the more thoroughly studied population of neurons ($n = 19$), we compared the change in spatial frequency cutoff with contrast for the high and low end of the spatial frequency tuning curve (Fig. 5). The absolute degree of change in the spatial frequency cutoff with contrast (low-high contrast) is, on average, smaller for the low-frequency cutoff (mean = 0.16) than for the high-frequency cutoff (mean = −0.49). The asymmetric effect of contrast on cutoff frequency suggests that the spatial frequency tuning is not well described by a Gabor filter with a varying envelope size. Furthermore, although the spatial frequency peaks vary little with contrast, this does not necessarily suggest that the spatial spread of the subunits is unaffected by contrast. A Gabor filter would predict that if the spatial frequency peak is unaffected by contrast, then the subunit size is also unaffected. The asymmetric change in spatial frequency bandwidth taken together with the relative contrast-invariance of the spatial frequency peak suggested that the spatial impulse response is more complex than a Gabor filter. As was shown in Fig. 1*F*, asymmetric changes in spatial frequency bandwidth coupled with little to no change in the spatial frequency peak can be explained by a model where the size and number of subunits both vary with contrast.

Spatial frequency selectivity and the iceberg effect

It has been suggested that neuronal response tuning may exhibit sharpening by thresholding through what is known as the iceberg effect (Carandini and Ferster 2000; Sompolinsky and Shapley 1997; Volgushev et al. 2000). Shifting the response gain of a given tuning curve around a fixed response threshold will cause responses along the tails of the tuning curve to fall below the firing rate threshold and become subthreshold. The remaining "tip of the iceberg" is effectively reduced in bandwidth (Fig. 6*A*). To determine whether such an iceberg effect can explain our results, low contrast responses were calculated on the assumption that the responses scale proportional to contrast and that there is a response threshold simulated from the empirical responses collected at high contrast. The high contrast responses were reduced in magnitude such that the peak responses at high and low contrast matched (with the spontaneous firing rate subtracted from both curves, Fig. 6*D*). This was accomplished by taking the difference

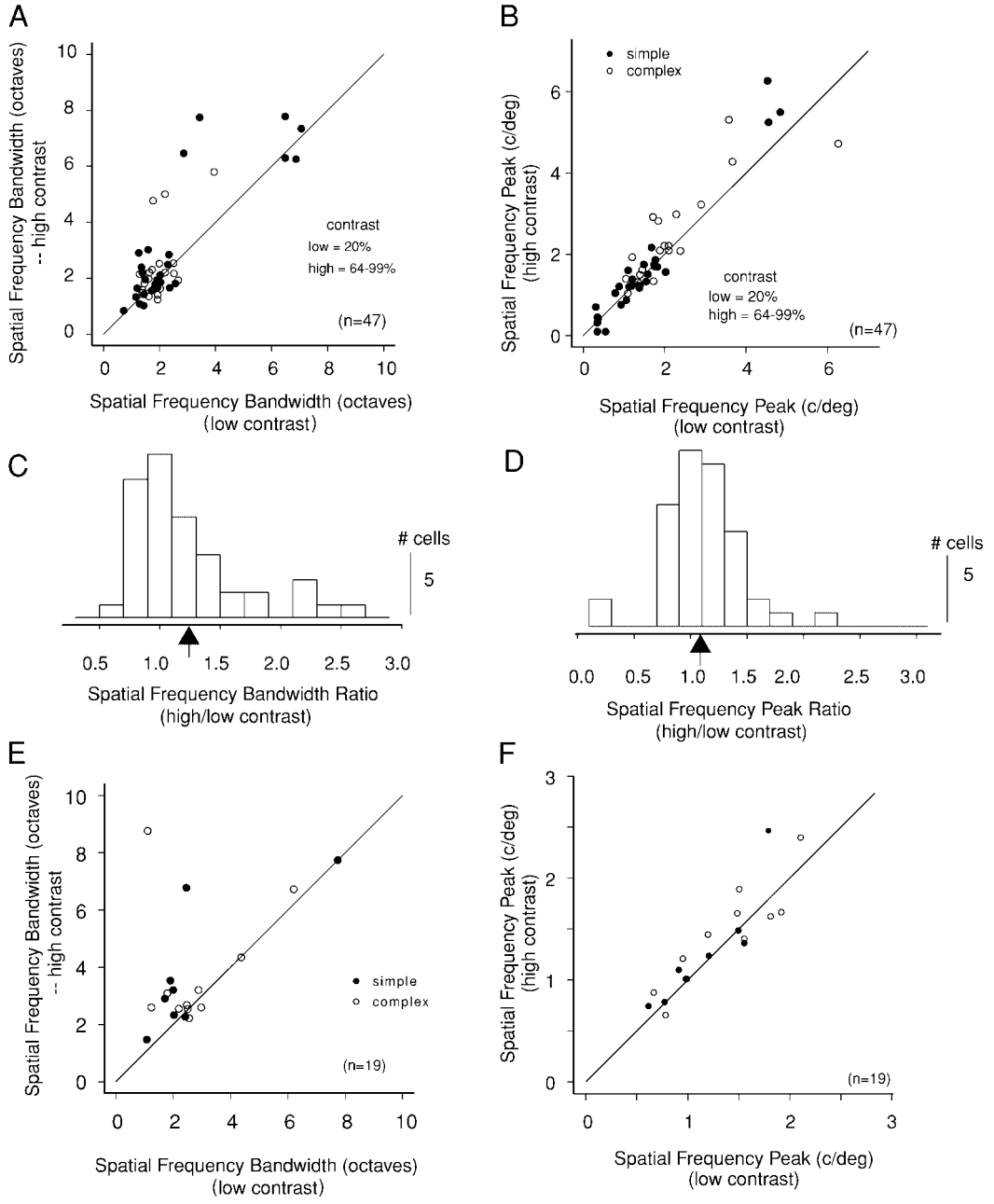

FIG. 3. Spatial frequency tuning at low and high contrast. From a database of 500 cells, we extracted spatial frequency tuning curves at fixed low (20%) and high (64–99%) contrasts. Only those responses where high contrast estimates are below saturation (<90% of the saturating response magnitude) are included ($n = 47$). Cells with peak spatial frequencies at low contrast that were below 0.4 cycles/° were excluded. Bandwidth estimates were estimated from the difference of Gaussian fits to the spatial frequency curves. Bandwidth is defined as the log ratio in octaves of the spatial frequencies at half-maximal response for the high cutoff to the low cutoff [$\log_2(SF_{high\ cutoff}/SF_{low\ cutoff})$]. *A*: simple cell estimates (●) were taken from the first harmonic amplitude responses and complex cell estimates (○) from the mean firing rate. *B*: peak spatial frequency tuning at low and high contrast for the same population. *C*: histogram of the bandwidth ratio (BW_{high}/BW_{low}). Vertical arrow indicates the population mean ($BW_{high}/BW_{low} = 1.24$), which is statistically different from unity (Wilcox ranked sum test, $P < 0.01$). *D*: histogram of the ratio of optimal spatial frequency ($Peak_{high}/Peak_{low}$). Population average ($Peak_{high}/Peak_{low} = 1.10$), indicated by vertical arrow, is not statistically different from unity (Wilcox ranked sum test, $P > 0.05$). The mean peak ratio for simple cells ($peak_{high}/peak_{low} = 1.05$) and complex cells ($peak_{high}/peak_{low} = 1.16$) are not significantly different from each other (Mann-Whitney test, $P > 0.05$). For an additional sample ($n = 19$), we collected spatial frequency tuning curves at contrasts that were tailored to each cell's contrast response function (see METHODS). *E*: estimates of spatial frequency bandwidth at low and high contrast taken from DOG fits to the spatial frequency tuning curves for simple cells (●) and complex cells (○) for this additional sample of neurons. The population mean ($BW_{high}/BW_{low} = 1.7$) is significantly greater than unity (Wilcox ranked sum test, $P < 0.001$). *F*: estimates of spatial frequency peak for low and high contrast. Mean peak ratio ($Peak_{high}/Peak_{low} = 1.10$) is not significantly different from unity (Wilcox ranked sum test, $P > 0.05$). Once again the mean peak ratio for simple cells ($peak_{high}/peak_{low} = 1.13$) and complex cells ($peak_{high}/peak_{low} = 1.08$) are not significantly different from each other (Mann-Whitney test, $P > 0.05$).

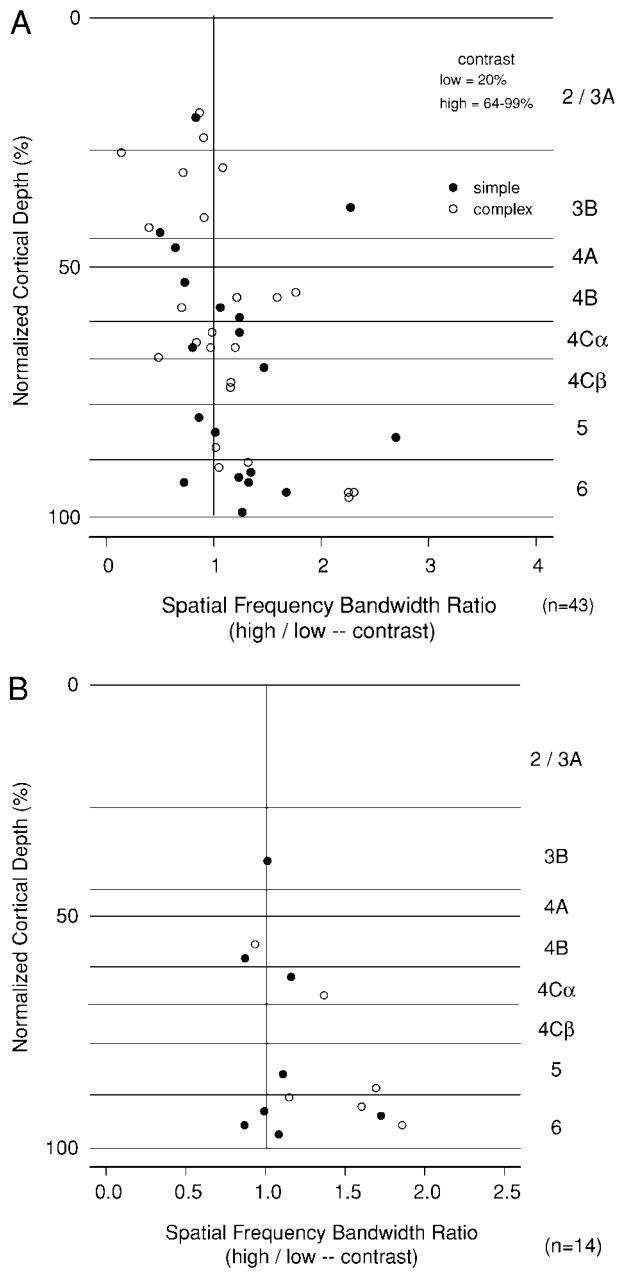

FIG. 4. Spatial frequency bandwidth ratio (high/low contrast) distribution across cortical layers. *A*: vertical line indicates unity ratio. Open circles indicate estimates for complex cells and filled circles for simple cells. Despite the small sample size ($n = 43$), there is more bandwidth change with contrast in the lower layers (mainly layer 6; layer 6 $BW_{low}/BW_{high} = 1.4$) and the mean is significantly different from unity (Wilcoxon test, $P < 0.001$). *Top layers* (layer 2/3, 3B, 4B) show a mean ratio that does not vary significantly from unity ($BW_{high}/BW_{low} = 0.98$, Wilcoxon test, $P > 0.05$). *B*: similar analysis for cells that were tested at contrasts tailored to each cell's contrast response function ($n = 14$). Simple cell estimates are shown as filled circles and complex cells as open circles. Although the sample is small ($n = 14$), it confirmed the impression that many cells in layer 6 change their spatial frequency bandwidth with contrast.

between the peak response at high − low contrast and subtracting this value from the high contrast response. Next, the responses were thresholded at zero. This new curve represents the tuning curve that would result from the iceberg effect, if we assume that the responses are scaled linearly with contrast and that there is a response threshold. From these new curves, we can estimate the hypothetical spatial frequency bandwidth at low contrast and compare it to the actual low contrast spatial frequency tuning curve.

We examined our population of neurons ($n = 19$) for the iceberg effect and found that most show bandwidth changes that are larger than the changes predicted by the iceberg effect. We compared the empirical responses collected at high and low contrast (Fig. 6, *B* and *C*) with responses simulated from the iceberg model. Figure 6*B* shows a sample neuron with a significant change in the bandwidth ratio for high to low contrast ($BW_{high}/BW_{low} = 1.3$, Fig. 6*B*). Normalizing the responses with respect to the peak response values at low and high contrast makes the change in bandwidth more obvious (Fig. 6*C*). To determine the degree of change in spatial frequency bandwidth resulting from the iceberg effect, we simulated the low contrast responses from the empirical high contrast estimates. First, the spontaneous firing rate was subtracted from the low and high contrast responses. This response can be normalized to its peak value to compare it to the empirical estimates at low contrast (Fig. 6*D*). The iceberg model does cause a reduction in the spatial frequency bandwidth (iceberg $BW_{low} = 1.9$, Fig. 6*D*) compared with the high contrast spatial frequency bandwidth ($BW_{high} = 2.2$, Fig. 6*D*). However, the bandwidth ratio at high to low contrast (BW_{high}/BW_{low}) is not as large for the iceberg model ($BW_{high}/BW_{low} = 1.15$, Fig. 6*D*) as it is for the ratio of the actual data ($BW_{high}/BW_{low} = 1.30$, Fig. 6*C*). Therefore, if there were a significant change in the cell's firing rate with contrast, it could explain part of the heightened selectivity for spatial frequency at low contrast. However, there is a significant portion of the bandwidth change that cannot be accounted for by the iceberg model. In addition, the iceberg gives a bandwidth reduction on the high and low frequency limbs of the tuning curve whereas the data most often shows a substantial change on the high spatial frequency limb but considerably less change on the low spatial frequency limb of the tuning curve. Because the spatial frequency peak does not change much with contrast, it is instructive to view this analysis on a linear scale where the high-frequency limb of

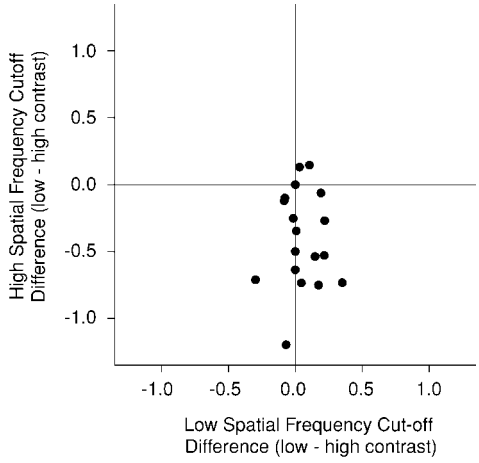

FIG. 5. Contrast-dependent change in spatial frequency cutoff. Spatial frequency cutoff difference at low − high contrast is shown for the high vs. low end of the spatial frequency tuning curve. Most of the points fall in the lower quadrants with a lesser tendency for the lower right quadrant, indicating that as contrast increases the high and low end of the spatial frequency tuning curve move away from the peak. However, changes to the high spatial frequency cutoff are greater, on average, than changes to the low frequency cutoff.

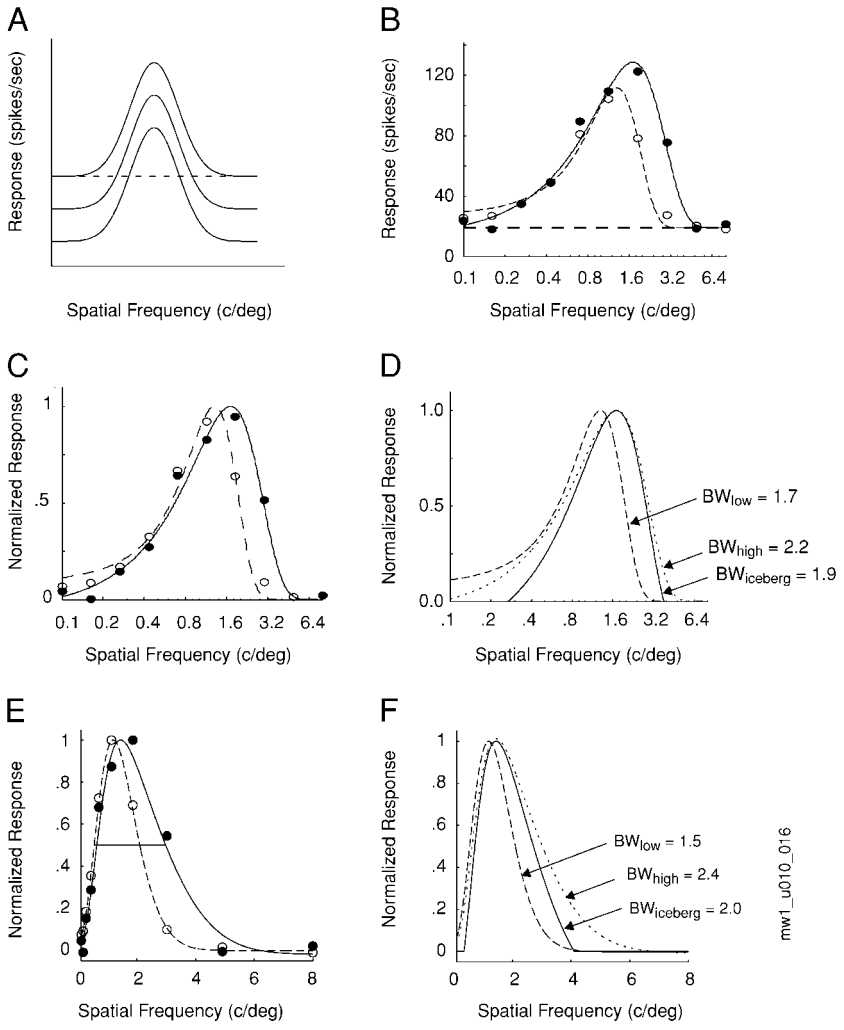

FIG. 6. Can a reduction in spatial frequency bandwidth be explained by a response threshold? *A*: in theory, reducing the response gain by a subtractive inhibition and thresholding the response will yield a smaller bandwidth for smaller responses. This is because small responses near the tails of the tuning curve become subthreshold after imposing a response threshold. *B*: spatial frequency tuning curves from the actual neuronal responses (spikes/s). Low contrast responses are shown as open circles and high contrast responses are shown as closed circles. Solid and dashed curves represent the DOG fits to the data for the high and low contrast responses, respectively. Horizontal dashed line is the spontaneous firing rate. *C*: same data shown in *B*, but with the responses normalized to the response peak to illustrate the contrast dependence of the spatial frequency bandwidth. Bandwidths are shown for the empirical estimates of spatial frequency tuning at low (BW_{low} = 1.7 octaves) and high contrast (BW_{high} = 2.2 octaves). *D*: illustration of the "iceberg" effect. A comparison between the actual low contrast responses (dashed line) and the simulated low contrast responses resulting from the iceberg effect (solid line). High contrast spatial frequency tuning curve is shown as a dotted line for comparison. Solid and dashed lines represent DOG fits to data for the empirical data at low contrast and the iceberg model simulations of the low contrast data, respectively. The iceberg model responses were produced by initially subtracting the spontaneous firing rate then the difference between the peak responses at high − low contrast was subtracted from the high contrast responses. Next the iceberg model responses were thresholded at 0. The resulting low contrast responses have a bandwidth ($BW_{iceberg}$ = 1.9) that is lower than the high contrast bandwidth (BW_{high} = 2.2), but not as small as the empirical estimates of the low contrast responses (BW_{low} = 1.7). Therefore the iceberg model cannot account for all of the bandwidth change observed in the data. *E* and *F*: same cells are shown on a linear scale with the bandwidth estimates shown as the full-width at half-height of the spatial frequency tuning curve and expressed as cycles/° rather than octaves.

the tuning curve is not logarithmically scaled (Fig. 6, *E* and *F*). The bandwidth estimates were also calculated as absolute differences between the spatial frequencies that produce 50% of the peak response on either side of the peak ($BW = SF_{high\ cutoff} - SF_{low\ cutoff}$). The results on the linear scale confirm that the iceberg effect cannot explain the complete amount of change in spatial frequency bandwidth with contrast ($BW_{high}/BW_{low} = 1.6$ for the actual data and $BW_{high}/BW_{low} = 1.2$ for the estimated bandwidth change in the iceberg model).

To determine whether or not the spatial frequency responses were subject to significant modification from a response threshold, we estimated spatial frequency tuning at contrast levels that are significantly above the contrast response threshold (≥2 SDs above the spontaneous firing rate and >10 spikes/s). There was no significant dependence on contrast of the spontaneous activity sampled during the blank runs that were interleaved between stimuli (data not shown). Therefore it is unlikely that a change in response threshold between contrast levels contributed significantly to enhanced selectivity through an iceberg effect.

Spatial frequency selectivity and spatial summation

Spatial frequency tuning predominantly depends on the size and number of subunits aligned orthogonal to the preferred orientation (DeAngelis et al. 1993). Therefore contrast-dependent changes in spatial summation along the receptive field width should have a direct effect on the spatial frequency tuning. Contrast-dependent changes in length summation do not relate directly to spatial frequency tuning. Increasing subunit length might sharpen orientation tuning while leaving spatial frequency tuning unaffected. For a representative neuron that displays reduction of the spatial frequency bandwidth at low contrast (Fig. 7*A*), we show the contrast dependence of length and width summation. Although there is no difference in the optimal length of summation with stimulus contrast (Fig. 7*B*), there is a significant decrease in the optimal width of summation at high contrast (Fig. 7*C*). Such a decrease in width summation at high contrast is consistent with an increase in spatial frequency bandwidth at high contrast. However, this particular cell displays a reduction only on the high-frequency end of the spatial frequency tuning curve. This example is representative of the population. Such a pattern of contrast-dependent variation of spatial frequency tuning cannot be explained solely by a change in the spatial envelope of a Gabor filter (Fig. 1). It is better described by a spatial filter where the central subunit expands at low contrast and also the strength of the flanking subunits increases at low contrast (see Fig. 1, *E* and *F*).

We compared the relative changes in spatial summation and

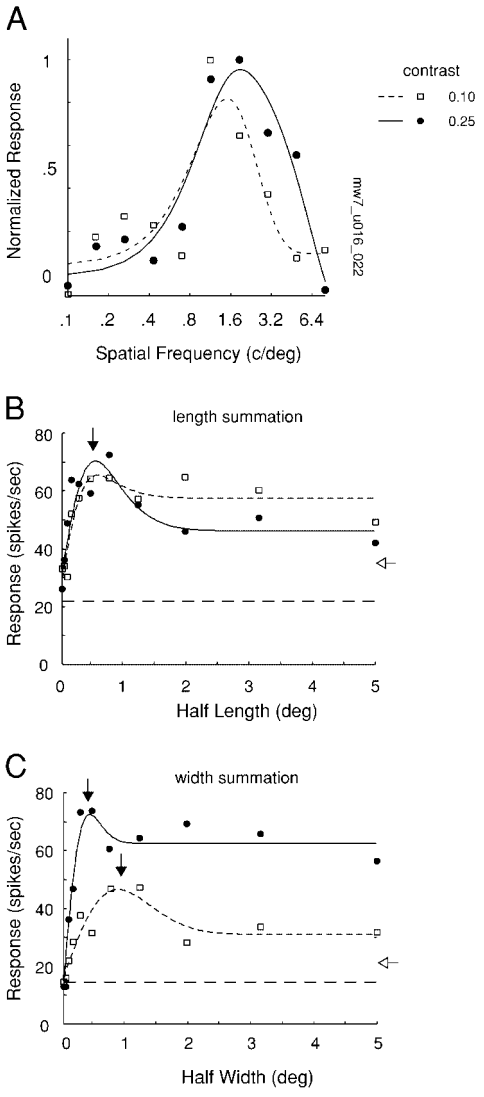

FIG. 7. Comparing contrast-dependent changes in spatial frequency tuning and spatial summation. Contrast-dependent changes in spatial frequency tuning correlate with changes in width summation rather than length summation. *A*: spatial frequency tuning at low and high contrast are shown for a representative neuron. Low contrast responses are shown as open circles and high contrast responses as filled circles. Curves fit to data are from a difference of Gaussians model. Solid curves correspond to high contrast and dashed curves to low contrast data. *B*: length summation profiles at low contrast (10%, open squares and dashed curves) and high contrast (25%, filled circles and solid curves) are shown for the same neuron shown above. Contrasts used in the spatial frequency tuning experiment and the summation experiments are identical. Curves fit to data are taken from the DOG model of spatial summation described in Sceniak et al. (2001). This is distinct from the DOG model that is used to fit the spatial frequency tuning functions in *A*. Vertical arrow indicates the optimal half-length of summation. For this example the optimal summation length does not change with contrast. Horizontal dashed line represents the spontaneous firing rate and the open horizontal arrow is placed 2 SD above the spontaneous rate. *C*: width summation profile for the same neuron. Vertical arrows indicate the optimal summation half-width at each contrast level. There is a clear reduction in the optimal half-width at high contrast.

spatial frequency bandwidth with contrast for area, length, and width summation (Fig. 8, *A–C*). For the sample of neurons studied ($n = 15$), area, length, and width summation each show a reduction in the optimal summation radius, half-length, or half-width, respectively, as contrast is increased (there are fewer cells in Fig. 8 than in Fig. 3*E*, because we were unable to gather data for all of the summation experiments on all of the original 19 cells). Contrast-dependent changes in width summation are significantly correlated with contrast-dependent changes in the spatial frequency tuning bandwidth ($R^2 = 0.54$,

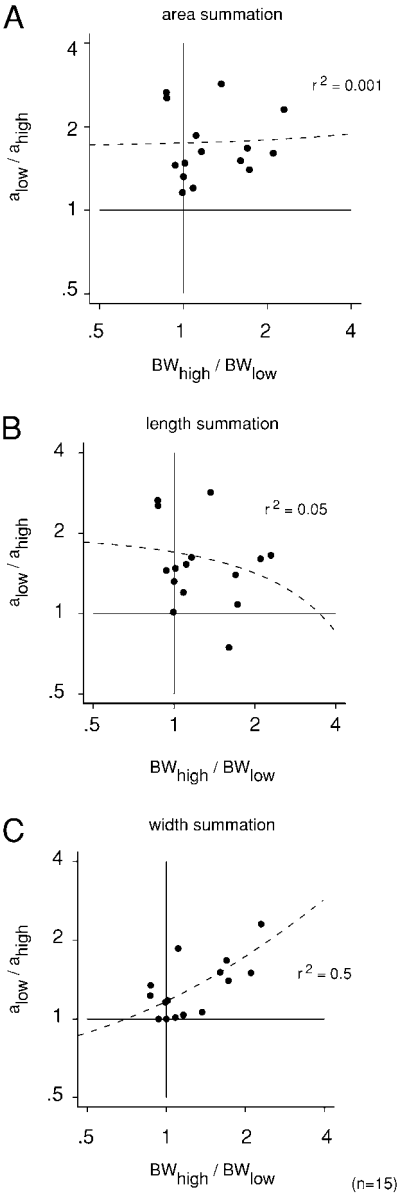

FIG. 8. Comparing contrast-dependent changes in spatial frequency bandwidth and spatial summation: area, length, and width summation. Change in spatial frequency bandwidth is expressed as the bandwidth at high to low contrast. Changes in the extent of spatial summation are shown as ratios of the excitatory space constant at low to high (a_{low}/a_{high}) contrast taken from fits to a integral difference of Gaussians model. *A*: contrast-dependent changes in circular area summation are compared with changes in the spatial frequency bandwidth. Solid horizontal and vertical lines indicate unity ratio and the dashed line is a linear regression fit to the data. There is no significant correlation with area changes estimated using circular grating patches. *B*: bandwidth changes show no significant correlation with the changes observed for length summation. *C*: across the sample of cells studied ($n = 15$), there is a significant correlation between changes in width summation and changes in spatial frequency bandwidth ($r^2 = 0.54$, $P < 0.01$). Bandwidth ratios, BW_{high}/BW_{low}, >1 indicate that spatial frequency bandwidth increases with increased contrast. Bandwidth increases at high contrast are correlated with decreases in extent of summation along the width axis ($a_{low}/a_{high} > 1$ indicate a reduction in the extent of summation with increased contrast).

$P < 0.01$, Fig. 8*C*). Although circular area summation and length summation both show significant change with contrast for the population of neurons studied ($n = 15$), changes in neither dimension are significantly correlated with contrast-dependent changes in the spatial frequency bandwidth (for area summation $R^2 = 0.001$ and for length summation $R^2 = 0.05$, Fig. 8, *A* and *B*). The lack of correlation between changes in area summation and spatial frequency bandwidth likely results from the fact that the circular-patch area experiments include summation along the length and width of the receptive field. Because cells that show changes in length summation are uncorrelated with changes in spatial frequency bandwidth with contrast, the area experiment includes such length summation effects as well as changes in width summation, resulting in a lack of correlation.

DISCUSSION

The major result of this paper is that reduction of stimulus contrast causes significant sharpening of spatial frequency tuning, and that this sharpening is correlated with expansion of spatial summation at low contrast.

Previously, we showed that spatial summation depends on contrast (Sceniak et al. 1999). This result is consistent with the findings of others (Kapadia et al. 1999). Spatial summation is, on average, 2.3 times greater at low contrast than at high contrast. These contrast-dependent changes in spatial summation can occur at both the ends and sides of the receptive field. Analysis with an empirical, DOG, model of spatial summation reveals that contrast-dependent changes in the optimal radius of summation are not correlated with contrast-dependent changes in surround strength. Therefore changes in the classical or excitatory receptive field size result from changes in excitation rather than from inhibitory sharpening.

It has been suggested that the spatial properties of the classical receptive field such as spatial frequency selectivity or orientation do not depend on stimulus contrast (Albrecht and Hamilton 1982; Bradley et al. 1987; Li and Creutzfeldt 1984; Movshon et al. 1978; Sclar and Freeman 1982; Sclar et al. 1990; Skottun et al. 1987). However, Bradley et al. (1987) did mention that the spatial frequency tuning bandwidth was systematically smaller at lower contrast. It is widely believed that contrast scales response magnitude with no differential effect on particular stimuli (Heeger 1992; Robson 1975). Response normalization has been proposed to account for contrast-invariant spatial tuning for properties such as orientation and spatial frequency (Carandini and Heeger 1994; Carandini et al. 1997; Heeger 1992; Tolhurst and Heeger 1997a,b).

If spatial summation is not contrast-invariant, then other spatial properties of the receptive field should be expected to change with spatial summation at different contrast levels. Spatial frequency selectivity and receptive field spatial spread (envelope) are inversely related. Using spatial frequency analysis, it has been shown that the inverse Fourier transform of the frequency response of complex cells gives spatial impulse responses that are similar in shape to simple cell's spatial weighting functions (Movshon et al. 1978b; Spitzer and Hochstein 1985a,b). This suggests that complex cells' spatial selectivity is dominated by subunits that are similar in structure to simple cells' spatial weighting functions. These subunits determine the dominant characteristics of the spatial frequency response function despite significant nonlinearities in summation (Movshon et al. 1978b).

To account for our findings about spatial frequency tuning and contrast, one must postulate that there are contrast-dependent changes in the spatial spread of individual receptive field subunits as well as the number and strength of flanking subunits. There is evidence that subthreshold excitatory regions surround the classical excitatory receptive field and may form the basis for this recruitment (Bringuier et al. 1999). What needs to be explained is that the change in spatial frequency bandwidth tends to be asymmetric with more bandwidth reduction occurring at the high spatial frequency cutoff. Also, there is little change with contrast in the location of the spatial frequency peak. A simulation of a receptive field composed of a DOG core with flanking Gaussian subunits (Fig. 1, *E* and *F*), predicts that asymmetric reductions in spatial frequency bandwidth biased for high frequencies might result from increases in the subunit size as well as an increase in the number of subunits within the receptive field.

We compared estimates of the change in optimal length and width summation with contrast to changes in the spatial frequency selectivity for each neuron across our population of V1 neurons. Changes in spatial frequency selectivity are significantly correlated with changes in the extent of summation along the receptive field width, but not length. A change in the spatial structure of the receptive field might explain the contrast-dependent change in spatial frequency selectivity reported here, but this change would only be related to changes in summation along the receptive field width. The correlation between changes in spatial frequency selectivity and width summation observed here are consistent with contrast-dependent spatial reorganization of the receptive field subunits.

Many investigators have found that orientation bandwidth does not vary much with contrast (including our own data that is not shown). The changes in receptive field structure that we needed to introduce into the model to explain the pattern of the spatial frequency results—the associated increase in envelope spread and carrier period of the Gabor or size and number of DOG subunits—are the kinds of changes that would tend to leave orientation bandwidth relatively unchanged. Thus, although contrast modulates spatial frequency bandwidth, because contrast affects width summation, it tends to leave orientation bandwidth invariant.

We thank Dr. Dario Ringach, E. Johnson, Dr. Isabelle Mareschal, and A. Henrie for help in data collection and L. Smith for assistance in the histological reconstruction work and help during physiology experiments.

This work was supported by National Eye Institute Grants EY-01472 and EY-08300, core Grant P30 EY-13079, and National Science Foundation-Learning and Intelligent Systems Grant IBN-9720305.

REFERENCES

ALBRECHT DG AND HAMILTON DB. Striate cortex of monkey and cat: contrast response function. *J Neurophysiol* 48: 217–237, 1982.

BONDS AB. Role of inhibition in the specification of orientation selectivity of cells in the cat striate cortex. *Vis Neurosci* 2: 41–55, 1989.

BRADLEY A, SKOTTUN BC, OHZAWA I, SCLAR G, AND FREEMAN RD. Visual orientation and spatial frequency discrimination: a comparison of single neurons and behavior. *J Neurophysiol* 57: 755–772, 1987.

BRINGUIER V, CHAVANE F, GLAESER L, AND FREGNAC Y. Horizontal propagation of visual activity in the synaptic integration field of area 17 neurons. *Science* 283: 695–699, 1999.

CARANDINI M AND FERSTER D. Membrane potential and firing rate in cat primary visual cortex. *J Neurosci* 20: 470–484, 2000.

CARANDINI M AND HEEGER DJ. Summation and division by neurons in primate visual cortex. *Science* 264: 1333–1336, 1994.

CARANDINI M, HEEGER DJ, AND MOVSHON JA. Linearity and normalization in simple cells of the macaque primary visual cortex. *J Neurosci* 17: 8621–8644, 1997.

DAUGMAN JG. Two-dimensional spectral analysis of cortical receptive field profiles. *Vision Res* 20: 847–856, 1980.

DAUGMAN JG. Spatial visual channels in the Fourier plane. *Vision Res* 24: 891–910, 1984.

DAUGMAN JG. Uncertainty relation for resolution in space, spatial frequency, and orientation optimized by two-dimensional visual cortical filters. *J Opt Soc Am [A]*. 2: 1160–1169, 1985.

DEANGELIS GC, OHZAWA I, AND FREEMAN RD. Depth is encoded in the visual cortex by a specialized receptive field structure. *Nature* 352: 156–159, 1991.

DEANGELIS GC, OHZAWA I, AND FREEMAN RD. Spatiotemporal organization of simple-cell receptive fields in the cat's striate cortex. I. General characteristics and postnatal development. *J Neurophysiol* 69: 1091–1117, 1993.

ELDRIDGE JL. A reversible ophthalmoscope using a corner-cube [proceedings]. *J Physiol (Lond)* 295: 1P–2P, 1979.

EMERSON RC, CITRON MC, VAUGHN WJ, AND KLEIN SA. Nonlinear directionally selective subunits in complex cells of cat striate cortex. *J Neurophysiol* 58: 33–65, 1987.

FIELD DJ AND TOLHURST DJ. The structure and symmetry of simple-cell receptive-field profiles in the cat's visual cortex. *Proc R Soc Lond B Biol Sci* 228: 379–400, 1986.

GLEZER VD, TSHERBACH TA, GAUSELMAN VE, AND BONDARKO VM. Linear and non-linear properties of simple and complex receptive fields in area 17 of the cat visual cortex. A model of the field. *Biol Cybern* 37: 195–208, 1980.

HAWKEN MJ AND PARKER AJ. Spatial properties of neurons in the monkey striate cortex. *Proc R Soc Lond B Biol Sci* 231: 251–288, 1987.

HAWKEN MJ, PARKER AJ, AND LUND JS. Laminar organization and contrast sensitivity of direction-selective cells in the striate cortex of the Old World monkey. *J Neurosci* 8: 3541–3548, 1988.

HAWKEN MJ, SHAPLEY RM, AND GROSOF DH. Temporal-frequency selectivity in monkey visual cortex. *Vis Neurosci* 13: 477–492, 1996.

HEEGER DJ. Normalization of cell responses in cat striate cortex. *Vis Neurosci* 9: 181–197, 1992.

HEGGELUND P. Receptive field organization of complex cells in cat striate cortex. *Exp Brain Res* 42: 90–107, 1981.

JONES JP AND PALMER LA. An evaluation of the two-dimensional Gabor filter model of simple receptive fields in cat striate cortex. *J Neurophysiol* 58: 1233–1258, 1987.

KAPADIA MK, WESTHEIMER G, AND GILBERT CD. Dynamics of spatial summation in primary visual cortex of alert monkeys. *Proc Natl Acad Sci USA* 96: 12073–12078, 1999.

KULIKOWSKI JJ, MARCELJA S, AND BISHOP PO. Theory of spatial position and spatial frequency relations in the receptive fields of simple cells in the visual cortex. *Biol Cybern* 43: 187–198, 1982.

LEVITT JB AND LUND JS. Contrast dependence of contextual effects in primate visual cortex. *Nature* 387: 73–76, 1997.

LI CY AND CREUTZFELDT O. The representation of contrast and other stimulus parameters by single neurons in area 17 of the cat. *Pflügers Arch* 401: 304–314, 1984.

MARCELJA S. Mathematical description of the responses of simple cortical cells. *J Opt Soc Am* 70: 1297–1300, 1980.

MERRILL EG AND AINSWORTH A. Glass-coated platinum-plated tungsten microelectrodes. *Med Biol Eng* 10: 662–672, 1972.

MOVSHON JA, THOMPSON ID, AND TOLHURST DJ. Receptive field organization of complex cells in the cat's striate cortex. *J Physiol (Lond)* 283: 79–99, 1978a.

MOVSHON JA, THOMPSON ID, AND TOLHURST DJ. Spatial and temporal contrast sensitivity of neurones in areas 17 and 18 of the cat's visual cortex. *J Physiol (Lond)* 283: 101–120, 1978b.

OHZAWA I, SCLAR G, AND FREEMAN RD. Contrast gain control in the cat's visual system. *J Neurophysiol* 54: 651–667, 1985.

ROBSON JG. Receptive fields: neural representation of the spatial and intensive attributes of the visual image. In: *Handbook of perception: V. Seeing*, edited by Carterette EC and Freidman MP. New York: Academic Press, 1975, p. 81–116.

SCENIAK MP, HAWKEN MJ, AND SHAPLEY R. Visual spatial characterization of macaque V1 neurons. *J Neurophysiol* 85: 1873–1887, 2001.

SCENIAK MP, RINGACH DL, HAWKEN MJ, AND SHAPLEY R. Contrast's effect on spatial summation by macaque V1 neurons. *Nat Neurosci* 2: 733–739, 1999.

SCLAR G AND FREEMAN RD. Orientation selectivity in the cat's striate cortex is invariant with stimulus contrast. *Exp Brain Res* 46: 457–461, 1982.

SCLAR G, MAUNSELL JH, AND LENNIE P. Coding of image contrast in central visual pathways of the macaque monkey. *Vision Res* 30: 1–10, 1990.

SKOTTUN BC, BRADLEY A, SCLAR G, OHZAWA I, AND FREEMAN RD. The effects of contrast on visual orientation and spatial frequency discrimination: a comparison of single cells and behavior. *J Neurophysiol* 57: 773–786, 1987.

SOMPOLINSKY H AND SHAPLEY R. New perspectives on the mechanisms for orientation selectivity. *Curr Opin Neurobiol* 7: 514–522, 1997.

SPITZER H AND HOCHSTEIN S. A complex-cell receptive-field model. *J Neurophysiol* 53: 1266–1286, 1985a.

SPITZER H AND HOCHSTEIN S. Simple- and complex-cell response dependences on stimulation parameters. *J Neurophysiol* 53: 1244–1265, 1985b.

SPITZER H AND HOCHSTEIN S. Complex-cell receptive field models. *Prog Neurobiol* 31: 285–309, 1988.

STORK DG AND WILSON HR. Do Gabor functions provide appropriate descriptions of visual cortical receptive fields? *J Opt Soc Am [A]* 7: 1362–1373, 1990.

SZULBORSKI RG AND PALMER LA. The two-dimensional spatial structure of nonlinear subunits in the receptive fields of complex cells. *Vision Res* 30: 249–254, 1990.

TOLHURST DJ AND HEEGER DJ. Comparison of contrast-normalization and threshold models of the responses of simple cells in cat striate cortex. *Vis Neurosci* 14: 293–309, 1997a.

TOLHURST DJ AND HEEGER DJ. Contrast normalization and a linear model for the directional selectivity of simple cells in cat striate cortex. *Vis Neurosci* 14: 19–25, 1997b.

VOLGUSHEV M, PERNBERG J, AND EYSEL UT. Comparison of the selectivity of postsynaptic potentials and spike responses in cat visual cortex. *Eur J Neurosci* 12: 257–263, 2000.

WALLIS G. Linear models of simple cells: correspondence to real cell responses and space spanning properties. *Spat Vis* 14: 237–260, 2002.